

The Flux One Magnetic Navigation System: A Preliminary Assessment for Stent Implantation

Christoff M. Heunis ¹, Bruno Silva, Giulia Sereni ², Martijn C.W. Lam, Besma Belakhal, Arold Gaborit, Bryan Wermelink, Bob R.H. Geelkerken, and Sarthak Misra ³, *Senior Member, IEEE*

Abstract—Minimally-invasive surgery (MIS) for stent implantation is a complex procedure requiring specialized instruments. It often leads to prolonged patient recovery, and interrupted operations due to incorrect instrument selection and complex anatomy. This study presents a novel magnetic navigation system that addresses these challenges by using magnetic fields and computed tomography imaging to precisely navigate minimally-invasive surgical guidewires. The system is designed based on consultations with surgeons, and analysis of technical and clinical requirements of stent implantation procedures. Results from a human-in-the-loop case study with eleven operators indicate a 47% reduction in guidewire navigation times, while successfully reaching all predetermined luminal targets. The clinical relevance, usability, and operator satisfaction are also measured using a user experience questionnaire, and interviews and showed positive results. Compared to conventional, manual guidewire navigation, the magnetic navigation system has the potential to significantly impact the efficiency of the clinical workflow and improve complex endovascular aortic repair procedures.

Index Terms—Medical robots and systems, surgical robotics: planning, surgical robotics: steerable catheters/needles.

Manuscript received 15 February 2023; accepted 13 June 2023. Date of publication 23 June 2023; date of current version 26 July 2023. This letter was recommended for publication by Associate Editor M. Tavakoli and Editor J. Burgner-Kahrs upon evaluation of the reviewers' comments. This work was supported in part by the European Research Council (ERC) under the European Union's Horizon 2020 Research and Innovation Program, ERC Proof of Concept under Grant 966703 – Project RAMSE and in part by an unrestricted research grant from the Pioneers in Health Care Innovation Fund, established by the University of Twente, Saxion University of Applied Sciences, Medisch Spectrum Twente, ZiekenhuisGroep Twente, Deventer Hospital, and Reggeborgh BV. (Corresponding author: Christoff M. Heunis.)

Christoff M. Heunis, Bruno Silva, Giulia Sereni, Martijn C.W. Lam, Besma Belakhal, and Arold Gaborit are with Surgical Robotics Laboratory, Department of Biomechanical Engineering, University of Twente, 7500 AE Enschede, The Netherlands (e-mail: c.m.heunis@utwente.nl; bruno.daniel@tecnico.ulisboa.pt; g.sereni@utwente.nl; martijnlam@live.nl; besma.belakhal@tuhh.de; arold06@outlook.fr).

Bryan Wermelink and Bob R.H. Geelkerken are with Multi-Modality Medical Imaging Group, Science and Technology Faculty, University of Twente, 7500 AE Enschede, The Netherlands, and also with the Department of Vascular Surgery, Medisch Spectrum Twente, 7512 KZ Enschede, The Netherlands (e-mail: b.wermelink@utwente.nl; r.h.geelkerken@utwente.nl).

Sarthak Misra is with Surgical Robotics Laboratory, Department of Biomechanical Engineering, University of Twente, 7500 AE Enschede, The Netherlands, also with Surgical Robotics Laboratory, Department of Biomedical Engineering, University of Groningen, 9713 GZ Groningen, The Netherlands, and also with Surgical Robotics Laboratory, Department of Biomedical Engineering, University Medical Centre Groningen, 9713 GZ Groningen, The Netherlands (e-mail: s.misra@utwente.nl).

This letter has supplementary downloadable material available at <https://doi.org/10.1109/LRA.2023.3289108>, provided by the authors.

Digital Object Identifier 10.1109/LRA.2023.3289108

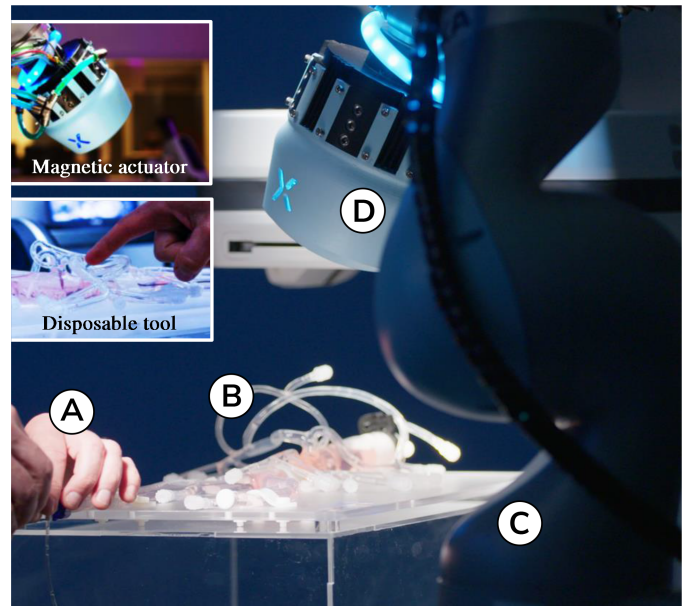


Fig. 1. This study introduces the development of a novel mobile magnetic navigation system (Flux One) for fenestrated endovascular aortic repair (f-EVAR) interventions. (A) A vascular surgeon inserts a magnetic J-tip guidewire into an aortic phantom (B). A collaborative, semi-autonomous serial link robot (C) positions an electromagnetic coil (D) in the workspace to assist the surgeon. A commercial fluoroscopy imaging modality provides real-time visual feedback of the position of the guidewire to the surgeon.

I. INTRODUCTION

EVERY year, 17.7 million deaths are attributed to cardiovascular disease (CVD) [1]. Atherosclerosis, a process weakening the arterial wall, is a common cause of CVD and increases the risk of developing an abdominal aortic aneurysm (AAA). Fenestrated endovascular aortic repair (f-EVAR) interventions are primarily used to treat AAA, which cannot be treated with traditional open surgical repair or standard EVAR. It involves placing a patient-specific endovascular stent graft in the aorta to isolate and reinforce the aneurysm. Aortic repair is the only treatment for AAA [2]. Particularly for stent implantation, intravascular guidewires play a crucial role in the endovascular treatment of CVD [3]. Such guidewires are necessary for accessing and navigating through various luminal structures.

Conventional guidewire insertion and placement procedures face two main issues: human error during risk assessment and complexity of patient anatomy [4], [5]. Evaluating patient blood vessel geometry often leads to selecting the wrong guidewire,

which occurs in 65% of cases [6]. This human error can result in incorrect instrument selection, potentially leading to prolonged recovery for the patient [7]. Surgeons consider patient anatomy complex 80% of the time, mainly due to fenestrations, necessitating specialized instruments, and increasing the risk of perforation, leading to higher morbidity and mortality rates [8].

In order to enhance the safety of guidewire interventions compared to manual interventions, various supporting systems have been presented, categorized as robotic-push or magnetic-pull actuation types [9]. Robotic-push systems allow surgeons to operate remotely from radiation sources using tendon-driven navigation [10], [11]. For example, the CorPath 200/GRX systems (Corindus Vascular Robotics, Middlesex County, USA) are designed to control guidewires during a procedure using tendons. However, they are reportedly limited in navigating through tortuous vessels due to guidewire deformation and friction [12]. The Magellan system utilizes a combination of robotic manipulation and a sheath-based approach combined with tendon-driven navigation. Nevertheless, it cannot perform distal movements due to its inability to rotate the guidewire [13].

On the other hand, magnetic-pull systems are becoming popular for endovascular treatment. For instance, the Niobe (Stereotaxis, St. Louis, USA) and the CGCI (Magnetecs, Inglewood, USA) systems, which are primarily for the treatment of cardiac arrhythmias [14]. Other magnetic systems, like the CardioMag (MultiScale Robotics Lab, ETH Zurich, Switzerland) [15], have also been successfully introduced for pre-clinical vascular interventions, exhibiting a wide range of achievable magnetic fields. However, these systems must be positioned around the entire body of a patient in order to generate the required fields, which impedes the use of a conventional fluoroscope and easy patient access. The MagHead system (Nanoflex Robotics, Zurich, Switzerland) has been developed specifically for pre-clinical use in neurovascular surgeries [16] to allow for such patient access. This system utilizes stationary external magnets placed in the operating room (OR) to establish a magnetic field over the upper torso of a patient. This system holds great promise; however, it is limited in providing the surgeon with direct interaction with guidewires, depriving them of tactile feedback. This limitation makes it difficult to accurately sense the forces and pressures applied to arteries during surgery. This can lead to tissue perforation and suboptimal outcomes [17].

This study presents the development and validation of the Flux One system, a mobile shared-control system that overcomes the limitations of current magnetic navigation systems from both an accessibility and control perspective (Fig. 1). The system is suitable for navigation in the entire peripheral vasculature model without the large footprint of the Niobe, CGCI, CardioMag, or MagHead systems. In contrast to tele-operative systems, the Flux One system enables the surgeon to operate directly on the patient while receiving real-time robotic assistance. The system's ability to pull guidewires magnetically allows for easier navigation through tortuous vessels than robotic-push systems. In contrast, the capability to rotate the guidewire tip directly allows for precise distal movements. The Flux One universal connector is designed with a magnetic guidewire, providing greater flexibility than push systems that require proprietary sheaths. Unlike current magnetic pull systems with static coils,

TABLE I
FLUX ONE SYSTEM IS DEVELOPED BASED ON CLINICAL REQUIREMENTS (THE NEEDS OF END-USERS AND PATIENTS) FOR FENESTRATED ENDOVASCULAR AORTIC REPAIR (F-EVAR) INTERVENTIONS

| Clinical/technical needs | Technical specification | Description |
|----------------------------------------------------------------------------------------------------------------------------------------------------------------------------------------------------------|------------------------------------------------------------------------------------------------------------------------------------------------------------------------------------------------|------------------------------------------------------------------------------------------------------------------------------------------------|
| The operator needs to be able to move an electromagnetic coil accurately and precisely above the body of the patient. | Movement accuracy and precision must be within ± 10 mm. | The system can precisely position the electromagnetic coil as needed to provide effective treatment at the arterial fenestration. |
| The surgeon should be able to deflect a magnetic J-tip guidewire in several angles towards fenestrations. | Field strength of at least 20 mT within minimum and maximum bounds of 50-300 mm [24]. | The electromagnetic field generated by the coil is strong enough to provide effective treatment within the required distance range. |
| The (anti)-Trendelenburg range of tilt angles affects the operating area. The navigation system must be able to operate within the limited space and positioned in conjunction with a fluoroscopy C-arm. | Based on the Artis Pheno (Siemens Healthineers), these ranges should be accounted for: Maximum width and length of 72 cm, maximum height of 78 cm, and compatibility with C-arm 'no-fly' zone. | This specification ensures that the system can be easily positioned in a medical facility and does not interfere with other medical equipment. |
| The surgical staff must be able to operate the navigation system with ease. | System must have clear and concise instructions for use. | Healthcare providers can easily and safely use the system to provide effective treatment. |
| The navigation system must be easy to transport and should not be too heavy. | Maximum weight of 150 kg and compact design for easy transport. | The system is easy to move and should eliminate the need for reinforced floors and elevator platforms. |
| The surgical staff must be able to use the navigation system frequently. | System must be durable and designed for frequent use. | The system can withstand frequent use and transport without breaking down or requiring frequent repairs. |
| The navigation system must not collide with a patient's torso or with the operator while being used. | Incorporate a robot virtual safety barrier (VSB) above and on the sides of the patient. | The system provides a safe treatment environment for patients and healthcare providers. |
| The navigation system should have the potential to reduce intervention times and improve clinical workflow. | A combination of intuitive interfaces need to be integrated with the system. | Healthcare providers can easily and effectively operate the system while utilizing benefits of shared control. |

such as the MagHead, Niobe, or the CGCI system, the Flux One system features a robotically-actuated electromagnetic coil that allows for reaching the patient from one or multiple angles without requiring repositioning. This accessibility is critical for effective fluoroscopy and quick access to the patient in case of an emergency. The controlled adaptability of the Flux One system leads to improved accuracy and reduced risk of complications during surgical procedures. Specifically, the system offers higher fields (up to 60 mT) [18] than the MagHead system (up to 20 mT) [16]. The robotically-actuated coil can be programmed to apply different levels of magnetic force and deflection to the guidewire, which can be tailored to the patient's specific needs and procedure. Compared to systems utilizing permanent magnets [19], [20], the Flux One system offers modulation of magnetic field strength and direction. This capability allows for the ease of changing guidewire deflection angles without the need to rotate the coil or change its pose.

This letter is organized as follows: Section II describes the development of the navigation system informed by technical and clinical needs. The Flux One system architecture, design, and control framework are explained. Furthermore, the principles of operation, including surgical planning and perioperative procedure, are outlined. In Section III, we test the feasibility and effectiveness of the proposed system. Section IV summarizes the results, focusing on the efficiency and user experience of the system. Finally, Section V concludes this letter and provides directions for future work.

TABLE II

IN THIS STUDY, A CUSTOM MAGNETIC GUIDEWIRE IS DESIGNED BASED ON CLINICAL REQUIREMENTS FOR FENESTRATED ENDOVASCULAR AORTIC REPAIR (F-EVAR) INTERVENTIONS

| Clinical/technical need | Technical specification | Description |
|-------------------------------------------------------------------------------------------------------|--------------------------------------------------------------------------------------------------------------------------------|-----------------------------------------------------------------------------------------------------------------------------|
| The guidewire must be able to navigate through small and tight spaces, such as the renal arteries. | The guidewire must have a diameter of 2mm and the distance from the tip to the end of the wire should be less than 35 mm [27]. | These dimensions are important to ensure compatibility with the catheter and sheaths used for the renal and iliac arteries. |
| The guidewire must be able to navigate through complex and tortuous anatomy with high flexibility. | The guidewire should have an angle of curvature of up to 122°, which is the take-off angle of the iliac arteries. | Guidewire can navigate through tortuous vessels while minimizing the risk of vessel damage. |
| The guidewire must be able to respond the mechanical forces applied during navigation and deployment. | The guidewire should be embedded with a magnetic element with a remnant magnetization of 1.29 – 1.32T [21]. | These specified magnetic forces ensure the guidewire is deflected to the required angles using the external magnet. |
| The magnetic guidewire must be compatible with a variety of medical devices and instruments. | The magnetic guidewire must have a universal connector and be able to fit through standard catheters and sheaths. | The magnetic guidewire must be used with existing medical devices and techniques. |

II. THE FLUX ONE SYSTEM

This section discusses the technical and clinical challenges of minimally-invasive stent implantation procedures. Moreover, we discuss and how a semi-autonomous system prototype, the Flux One system, is able to overcome these challenges during a guidewire intervention.

A. Clinical Needs

To address the challenges and limitations encountered by surgeons during minimally-invasive vascular stent implantation procedures, particularly in complex anatomy cases, Flux One (Table I) and its complementary guidewire (Table II) are developed. Conventionally, surgeons control the proximal insertion and rotation of guidewires during stent procedures. The Flux One magnetic navigation solution aims to reduce the mental workload of the surgeon with one of these aspects, allowing them to focus solely on insertion.

In general, f-EVAR involves creating a custom-made stent graft designed to fit the patient's unique anatomy, which may involve incorporating one or more fenestrations to accommodate the renal arteries or other vital side branches. The number of fenestrations required will depend on the extent of the aneurysm and the location of the branches that need to be preserved. On average, f-EVAR procedures may involve sleeving one to four fenestrations in visceral side branches with guidewires [4]. However, surgeons may face challenges in selecting the appropriate guidewire to navigate the patient's vasculature and lesion, and may need to alter their choice during the procedure [21]. Using multiple guidewires can result in longer intervention time and increase the risk of inefficacy. To mitigate this, we propose using a single magnetic guidewire with multiple deflection

angles spanning from -135° to 135° and implementing a pre-operative planning framework based on 3D patient vasculature segmentation.

B. The System Interfaces

The system offers four control interfaces to the operator that provide various options for interaction with the system, based on their preference and task requirements:

The automatic positioning of the Flux One robot end-effector is established through a customized mechanical controller. This controller enables the operator to press pushbuttons to automatically send the robot to pre-defined poses. This controller is suitable for prescribing these poses without requiring expertise in robotics and can, therefore, be used by untrained, non-technical personnel. Next, a graphical user interface (GUI) is suitable for tasks that require general input commands and can be controlled through a touchscreen display. This interface is easy to use and does not require special training or expertise. Furthermore, it is compatible with conventional OR monitors, requiring no extra training. A wireless control interface (SpaceMouse, 3DConnexion Munich, Germany) allows the surgeon to safely and remotely control magnetic forces directly from the bedside. The wireless control interface is useful for tasks within confined spaces.

An off-the-shelf haptic interface (Force Dimension, Nyon, Switzerland) allows the operator to displace the robot end-effector in real-time through a high-level server-client library in MATLAB v2017b (Mathworks, Natick, USA). The off-the-shelf haptic interface is ideal for tasks that require real-time manipulation of the robot end-effector. Furthermore, the haptic device is utilized during small, accurate, and quick adjustments to improve the operator's ability to detect tissue resistance or incidental contact and ensure the robotic arm's safe movements during surgery.

Further components are integrated for the system to function. An electromagnetic coil (Flux Robotics B.V., Enschede, the Netherlands) is the key functional element of the robot, allowing it to guide and position disposable instrument tips at a 2 mm accuracy [22]. A KUKA LBR iiwa arm (KUKA, Augsburg, Germany) positions the coil and wirelessly steers a flexible disposable instrument within the human body. It has a horizontal reach of 830 mm, making it suitable to reach any patient extremity. All sub-components are integrated within the mobile trolley, adding to a total weight of 120 kg, and are powered by a single industrial power chord. The trolley allows individuals to transport the robotic arm between ORs, resulting in a mobile, transportable platform.

C. Surgical Planning

The system requires an actuation strategy for deflecting a guidewire into fenestrations. Each fenestration or opening through which the guidewire is to be deflected serves as one of $n \in \mathbb{N}$ poses for the coil. The objective is to ensure that the angle between the coil X-axis always points towards the arterial fenestration (Fig. 2). This implies that the coil is never parallel to the guidewire and can, therefore, apply a torque that deflects the

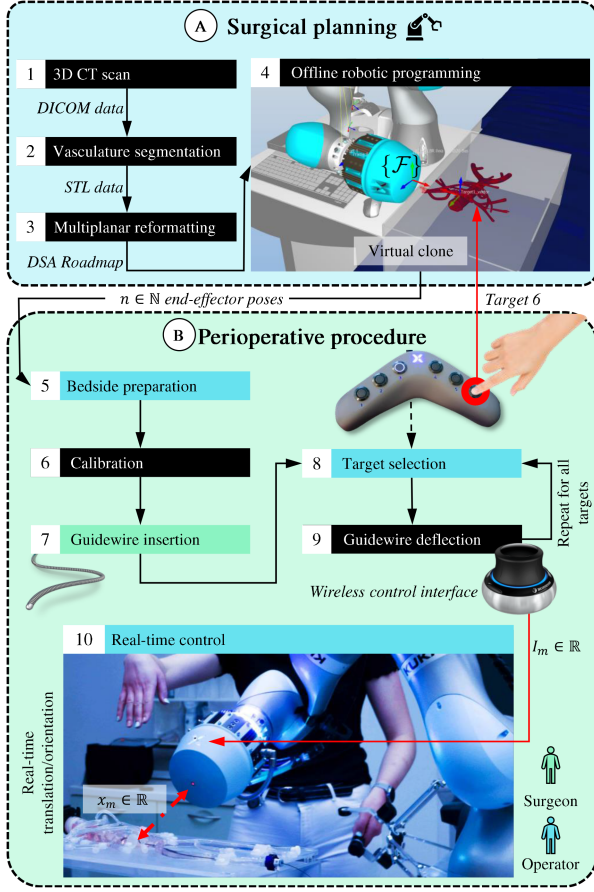


Fig. 2. The process of preparing the Flux One system for surgery. (A) A virtual clone of the entire system assists with defining the trajectories before the intervention occurs. The end-effector poses (n) are then digitally transferred to the system. (B) *Semi-autonomous control* - the system positions the coil in the workspace across the intended target. *Shared control* - an operator positions the coil at a distance ($x_m \in \mathbb{R}$) from the target. The surgeon controls the magnetic field strength by varying the current input ($I_m \in \mathbb{R}$).

guidewire. DICOM data taken from the patient's pre-operative 3D cone beam CT scan is segmented using proprietary software, which visualizes the target fenestrations for the guidewire. This data allows for the generation of the vectors pertaining to the 3D position and direction of a fenestration with respect to the main artery. The data is then loaded into a virtual model containing models of the navigation system and imaging equipment. The virtual 3D model simulates the surgery and plans the robot's trajectories based on a Policy Improvement with Path Integrals algorithm [23]. During surgical planning, the objective is to determine the end-effector frame ($\{\mathcal{F}\}$) trajectory of the robot that can perform its tasks with accuracy (i.e., reaching zones close to prescribed luminal targets) and without collisions.

End-effector poses are calculated using the following constraints: 1) the position of the fenestration, 2) the functional workspace of the coil, and 3) a virtual safety barrier (VSB). We define the position of the fenestration ($\mathbf{p}_f \in \mathbb{R}^3$), which is where the magnetic dipole ($\boldsymbol{\mu} \in \mathbb{R}^3$) of the embedded magnets will be located. The coil position ($\mathbf{p}_e \in \mathbb{R}^3$) should reside within a range defined by Table I:

$$r_{min} \leq \|\mathbf{p}_e - \mathbf{p}_f\| \leq r_{max}, \quad (1)$$

Algorithm 1: Coil Pose and Virtual Safety Barrier Generation.

Inputs:
 $\mathbf{p}_f \in \mathbb{R}^{3 \times n}$ \Rightarrow User-defined fenestration targets ($\mathbf{p}_{f_{i=1}}^n$)
 $\mathbf{c} \in \mathbb{R}^{3 \times n}$ \Rightarrow User-defined aortic centroids ($\mathbf{c}_{i=1}^n$)
 $\Psi_{CT} \in \mathbb{R}^{m \times 3}$ \Rightarrow DICOM model with m 3D points

Outputs:
 $\text{VSB} \in \mathbb{R}^{8 \times 3}$ \Rightarrow Virtual safety barrier around 3D model
 $\mathbf{S} = (x_{e_i}, \alpha_{e_i}, \theta_{e_i})_{i=1}^n$ \Rightarrow Set of poses composed of n spherical coordinates

- Initialization:
- $\mathbf{c}_p = \left[\frac{\sum \Psi_{CTx}}{m}, \frac{\sum \Psi_{CTy}}{m}, \frac{\sum \Psi_{CTz}}{m} \right]$ \Rightarrow Calculate centroid of 3D model: $[c_{\psi_x}, c_{\psi_y}, c_{\psi_z}]$
- for $j = 1: m$ do \Rightarrow Take the maximum distance of any point from the centroid in each direction (x, y, z). r_{min} is a safety margin
 - $d_x = \max(\text{abs}(\Psi_{CTx,j} - c_{\psi_x})) + r_{min}$
 - $d_y = \max(\text{abs}(\Psi_{CTy,j} - c_{\psi_y})) + r_{min}$
 - $d_z = \max(\text{abs}(\Psi_{CTz,j} - c_{\psi_z})) + r_{min}$
- $\text{VSB} = [(c_{\psi_x} - d_x, c_{\psi_y} - d_y, c_{\psi_z} - d_z), (c_{\psi_x} + d_x, c_{\psi_y} - d_y, c_{\psi_z} - d_z), (c_{\psi_x} - d_x, c_{\psi_y} + d_y, c_{\psi_z} - d_z), (c_{\psi_x} + d_x, c_{\psi_y} + d_y, c_{\psi_z} - d_z), (c_{\psi_x} - d_x, c_{\psi_y} - d_y, c_{\psi_z} + d_z), (c_{\psi_x} + d_x, c_{\psi_y} - d_y, c_{\psi_z} + d_z), (c_{\psi_x} - d_x, c_{\psi_y} + d_y, c_{\psi_z} + d_z), (c_{\psi_x} + d_x, c_{\psi_y} + d_y, c_{\psi_z} + d_z)]$
- while $i < n$ do \Rightarrow For each target in \mathbf{p}_f
 - 5 $\mathbf{w}_i = \mathbf{c}_i - \mathbf{p}_{f_i}$ \Rightarrow Calculate the normalized vector from the aorta centroid (\mathbf{c}_i) to the arterial fenestration (\mathbf{p}_{f_i})
 - 6 $\mathbf{u}_i = \frac{\mathbf{w}_i}{\|\mathbf{w}_i\|}$
 - 7 $\alpha_i = \text{atan2}(w_{i,y}, w_{i,x})$ \Rightarrow Calculate the angle (α_i) between the vector \mathbf{w}_i and the positive x -axis
 - 8 $\theta_i = \cos^{-1}\left(\frac{w_{i,z}}{\|\mathbf{w}_i\|}\right)$ \Rightarrow Calculate the angle (θ_i) between the vector (\mathbf{w}_i) and the positive z -axis
 - 9 $\mathbf{p}_{e_i} = \mathbf{p}_{f_i} - (\mathbf{u}_i \cdot \mathbf{p}_{f_i} - \mathbf{c}_i) \mathbf{u}_i$ \Rightarrow Calculate the coil position (\mathbf{p}_{e_i}) by projecting \mathbf{p}_{f_i} onto the plane perpendicular to \mathbf{u}_i , satisfying constraints in Eq. 1. β is a scaling factor to adjust the distance
 - 10 $\mathbf{p}_{e_i} \leftarrow \mathbf{p}_{e_i} + \beta \mathbf{u}_i$ \Rightarrow Calculate the spherical coordinates for the final pose
 - $x_{e_i} = \|\mathbf{p}_{e_i}\|$
 - $\alpha_{e_i} = \text{atan2}(p_{e_i,y}, p_{e_i,x})$
 - $\theta_{e_i} = \cos^{-1}\left(\frac{p_{e_i,z}}{x_{e_i}}\right)$
- $i + +$ \Rightarrow Increment i
- end

where $r \in \mathbb{R}$ is the distance between the coil position and the fenestration. The functional workspace of the coil is defined as a magnetic field ($\mathbf{B}(\mathbf{p}) \in \mathbb{R}^3$) at any point ($\mathbf{p} \in \mathbb{R}^3$) in space wherein a magnetic interaction occurs between the guidewire dipole and the field. This dipole will experience a wrench ($\mathbf{W}_\mu \in \mathbb{R}^6$) within this field:

$$\mathbf{W}_\mu = \begin{bmatrix} \mathbf{F}_\mu \\ \mathbf{T}_\mu \end{bmatrix} = \begin{bmatrix} \nabla(\boldsymbol{\mu}^T \mathbf{B}(\mathbf{p})) \\ \boldsymbol{\mu} \times \mathbf{B}(\mathbf{p}) \end{bmatrix}, \quad (2)$$

where $\mathbf{F}_\mu \in \mathbb{R}^3$ is a force and $\mathbf{T}_\mu \in \mathbb{R}^3$ is a torque component. Specifically, the coil should be perpendicular to the deflection axis of an axially-magnetized guidewire tip, resulting in maximum torque [24]. Finally, the coil position should respect any VSB vertices around the arteries. The VSB constraint is applied to ensure that the coil does not collide with the 3D model, as explained in Algorithm 1.

Reference frame transformations are calculated within the virtual clone, as depicted in Fig. 2. In accordance with the kinematic constraints of the robotic system, the virtual clone software then calculates trajectories between each target.

D. Perioperative Procedure

The perioperative procedure, as depicted in inset (B) of Fig. 2, involves first the automatic positioning of the coil, followed by shared control by an operator and surgeon. Shared control is established to drive the guidewire's bending (a change in the curvature) and its rotation about the axis perpendicular to its longitudinal axis. The operator uses the haptic interface if the end-effector needs to be adjusted. If, at any time, the movement of the robot violates the established VSB constraints, force feedback maintains constraint compliance [25]. In this case, the end-effector velocity ($\mathbf{V}_e \in \mathbb{R}^3$) between the start and end points of the end-effector position ($\mathbf{p}_e \in \mathbb{R}^3$) in frame $\{\mathcal{F}\}$ is used to compute the joint velocities ($\dot{\mathbf{q}} \in \mathbb{R}^{1 \times 7}$). The calculation of joint velocities is performed employing an inverse kinematics method in conjunction with the manipulator Jacobian ($\mathbf{J} \in \mathbb{R}^{7 \times 7}$):

$$\dot{\mathbf{q}} = \mathbf{J}^\dagger \mathbf{V}_e(\mathbf{p}_e). \quad (3)$$

The Jacobian is damped using the damped pseudo-inverse [26], (\mathbf{J}^\dagger), defined by:

$$\mathbf{J}^\dagger = \mathbf{J}^T (\mathbf{J}\mathbf{J}^T + \rho^2 \mathbf{I})^{-1}, \quad (4)$$

where ρ is the damping coefficient and $\mathbf{I} \in \mathbb{R}^{7 \times 7}$ denotes the identity matrix. Upon activation of the coil, the magnetic guidewire is deflected and the fenestration is entered.

III. EXPERIMENTS

This section presents the development steps to test and validate the system in a human-in-the-loop phantom case study. Furthermore, the performance and intuitiveness of the magnetic navigation system are evaluated, focusing on its ability to reduce intervention times.

A. Guidewire Prototype Test

To calculate the force required to achieve the desired deflection, we consider the magnetic properties of the guidewire magnets, guidewire tip flexibility, the magnetic properties of the coil, and the distance between the coil and the guidewire. In this study, the magnetic dipole should be aligned with the longitudinal axis to optimize the bending torque (\mathbf{T}_μ) of (2) for controlled fenestration navigation. We alter a commercial 32 in (0.81 mm) diameter J-tip guidewire (RadifocusT Guide Wire M Standard, Terumo Corp., Japan) by designing and integrating a magnetic tip (Fig. 3(a)) using finite element method software COMSOL Multiphysics (v5.5, COMSOL Inc., USA) [27]. The tip is optimized for minimal length while maintaining a fixed diameter of 2 mm and five Neodymium magnets (Supermagnete, Gottmadingen, Germany). The flexibility of the guidewire is constrained to be greater than 20° . The final design, with a tip length of 10 mm, shows a significant reduction in length compared to previous designs [28], [29]. The tip is coated with silicone rubber compound (Dragon SkinTM 20/0,9 kg, FormX, Amsterdam, the Netherlands) to ensure alignment of the magnets' dipoles. The angle of curvature is measured by fitting a circle to the curved portion of the guidewire and calculating the angle subtended by the arc. Furthermore, the field required to displace the tip from a fixed position is measured

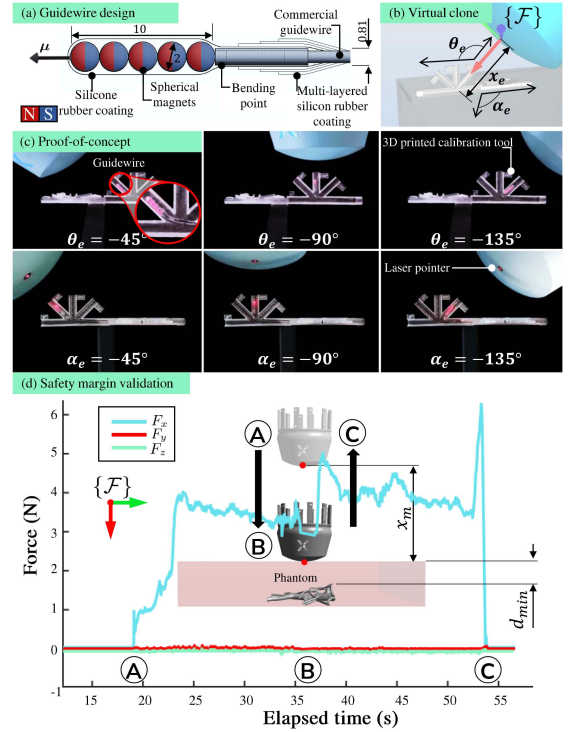


Fig. 3. Proof-of-concept design and validation: (a) The magnetic guidewire tip is designed based on Table II. All units are expressed in mm. (b) A virtual clone of the spherical end-effector and mock-up artery, visualizing its frame ($\{\mathcal{F}\}$), pose with coordinates (x_e , θ_e , and α_e), where x_e is the radial distance, θ_e is the polar angle, and α_e is the azimuthal angle. (c) Validation of the system calibration and guidewire efficacy. (d) End-effector safety margin validation. The end-effector is moved towards the phantom (from (A) to (B)) along a distance (x_m) and removed at (C).

using a three-axis teslameter (3MH3A-500MT Senis AG, Baar, Switzerland).

A preliminary experiment assesses the interaction between the magnetic guidewire and coil's magnetic field (Fig. 3(b) and (c)). The end-effector's maximum linear and angular velocity is set to $\mathbf{V}_e(\mathbf{p}_e) = 0.02$ m/s and $\omega_e = \pi/90$ rad/s, respectively, for safety reasons. The empirical virtual interaction force constraint is 4 N (Fig. 3(d)). A 3D-printed mock-up artery with six pre-defined angles is used to mimic channels with $\pm 45^\circ$, $\pm 90^\circ$, and $\pm 135^\circ$ orientations in horizontal and vertical planes. VSB constraints are validated to avoid collision with the phantom.

B. Guidewire Navigation Experiment

The system is first tested for CT compatibility since artifacts may affect the accuracy and quality of the CT images. To address this concern, the coil is directly positioned below the C-arm in a hybrid OR (Fig. 4) (TechMed Centre, University of Twente, Enschede, the Netherlands) and turned on. A technician (Siemens Healthineers) evaluated these images and confirmed that no artifacts would hinder the surgeon's workflow. A silicone-printed Abdominal Regional model based on actual patient CT data is used to conduct a mock-up instrumentation of the side branches of the aorta. The system is then positioned and calibrated using pre-determined landmarks of the phantom. Using the Artis Pheno software, a 2D X-ray image of the projected landmark pattern is then aligned with the corresponding points in the 3D

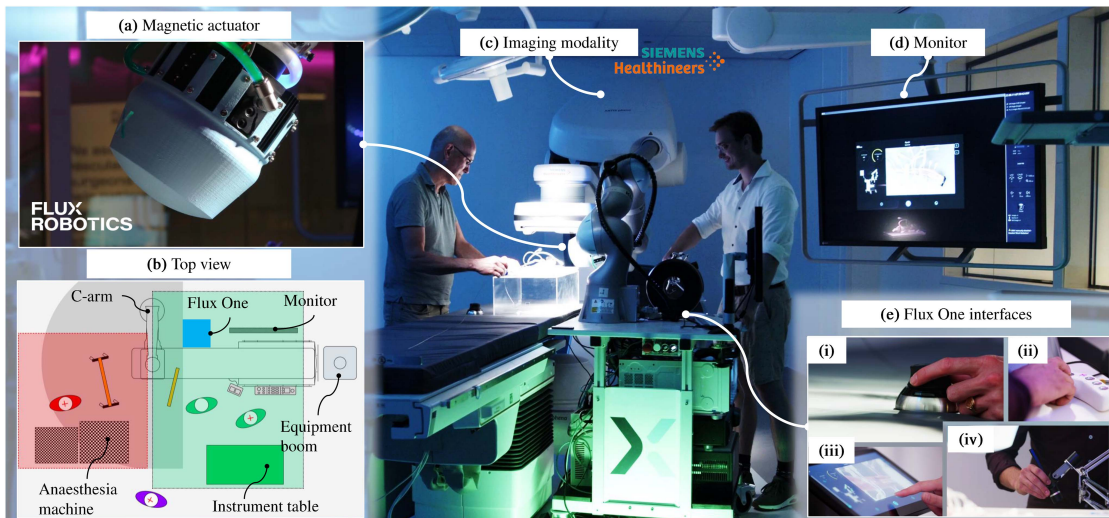


Fig. 4. The mobile Flux One system in a hybrid operating room (OR): (a) A liquid-cooled electromagnetic end-effector for magnetic guidewire deflection. (b) Congestion around the imaging table. **Green**: sterile, **red**: anesthesia, **purple oval**: circulatory nurse, **red oval**: anaesthesiologist, and **yellow**: radiation shields. (c) CT scanner for pre-operative planning and intra-operative guidance. (d) A monitor relaying real-time fluoroscopy images and the system status. (e) Four separate interfaces: (i) a wireless knob for navigating the guidewire tip; (ii) push buttons for positioning the robotic end-effector; (iii) a touch screen for operator interaction and clinical tasks; (iv) an Omega.6 haptic device for real-time coil positioning. Please refer to the accompanying video that describes the experimental setup and results.

scan. This registration process establishes the transformation matrix that maps the robot's reference frame to the phantom anatomy, enabling the robot to perform tasks opposite the correct arteries. The flow rate for the cooling system is set to 9.2 liters per minute to ensure a stable surface temperature (45 °C) of the coil.

A vascular surgeon with 20+ years of experience (Medisch Spectrum Twente, Enschede, the Netherlands) performs guidewire navigation using traditional (Case 1) and magnetic (Case 2) guidewires. The phantom targets include the coeliac artery and its branches, the superior mesenteric artery, the left renal artery, and the contralateral common iliac artery. The surgeon is requested to randomize the targets, to ensure no ensure minimal learning or familiarity with the procedure. Eleven participants (mean age 25 years, six male and five female) with no prior experience with human-machine interfaces (18% left-handed) are enrolled in Case 2. The duration of each intervention is recorded. System usability is then assessed with a System Usability Scale (SUS) and a User Experience Questionnaire measuring attractiveness, perspicuity, efficiency, dependability, stimulation, and novelty. Experiments are conducted between July and August 2022.

IV. RESULTS & DISCUSSION

This section presents the validation study results concerning the potential of the system to reduce intervention times. It discusses the impact of magnetic navigation on the field of guidewire navigation for stent implantations.

A. Case Study Comparison

The surgical procedure is initiated using a traditional guidewire. However, it encountered difficulties due to its inability to reach target 4 (the superior mesenteric artery). To overcome this challenge, an additional guiding catheter is employed.

All surgical targets are eventually reached during Case 1. The surgeon switched to the magnetic guidewire during the second procedure (Case 2) and successfully reached all targets without further interruptions or needing an additional guiding catheter. Target 4 demonstrates the most significant difference, with an average time of 22.7 s to be reached in Case 2, compared to 73 s in Case 1, reflecting a time reduction of 69%. The full-time procedure for each operator is shown in Fig. 5. In Case 2, procedure times are short, ranging between 11 and 37 s per target.

B. User Experience

Data collected from interviews are analyzed to identify patterns and themes related to the usability of the Flux One system. The System Usability Scale (SUS) and User Experience Questionnaire (UEQ) are utilized to collect operator ratings on various aspects of the system. The SUS comprises 10 questions on a 5-point Likert scale, while the UEQ includes 26 questions on a 7-point Likert scale. A composite SUS score is calculated from operator responses, providing an overall assessment of the system's usability. A total of 432 responses are analyzed and compared with interview data to determine system usability and overall satisfaction.

C. Main Findings and Limitations

By employing magnetic theory and a 7-degree-of-freedom (7DoF) semi-autonomous control system for surgical instruments, the handling time of guidewires during surgical procedures was reduced by 47% compared to traditional manual methods. The use of this system demonstrated high reliability with no recorded adverse events. The reduction in guidewire handling time achieved with this system is comparable to that achieved with the Magellan (37%) and CorPath (24%) systems [30]. The Flux One system scores well on efficiency, usability, and overall

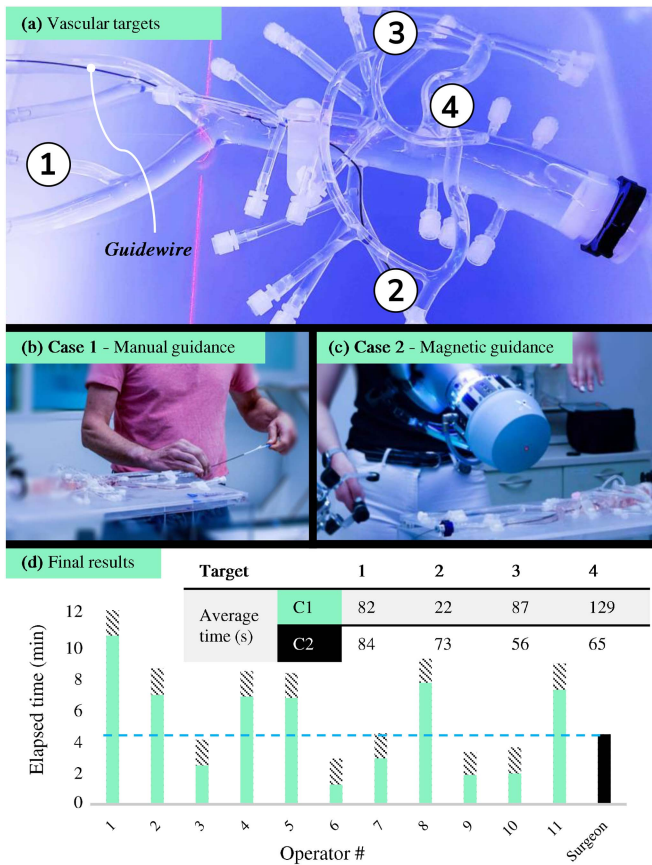


Fig. 5. (a) In this case study, a vascular phantom is used to represent several targets ①–④, to which a guidewire should be navigated. (b) A surgeon navigates a conventional guidewire manually (Case 1). (c) The Flux One system assists with navigating a magnetic guidewire (Case 2). (d) Comparison of total procedure times for reaching all targets. Green indicates the teleoperated durations of each operator relative to the surgeon. Black-shaded regions are taking the autonomous robot motion time during automatic positioning into account.

user experience with a mean SUS score of 80%. Compared to our previous work [18], the system is considered more intuitive in control by a surgeon, lightweight, and designed to be integrated with conventional ORs. Positive feedback from operators with no prior medical or robotics experience indicates the system’s ease of use and user-friendly interface design. Interviews suggest the need for a smaller system footprint. The system can improve surgical efficiency and patient outcomes by reducing mental workload and handling times. The shared control framework enables the surgeon to make informed decisions, addressing the problem of insufficient haptic feedback, and is valuable in complex or high-risk procedures. Previous studies support the use of autonomous and hands-on modes, where the former prioritizes accuracy and repeatability and the latter enables shared control between surgeon and robot while allowing for virtual constraints for added safety [31]. By prioritizing the human-in-the-loop factor, we can ensure that the surgeon is still an integral part of the procedure and that their craft and judgment are valued. The Flux One system’s calibration method is limited to immobile patients, requiring new tracking methods if the patient is repositioned during the procedure. The effective

DoF of the system is the manipulator and coil (7DoF) and the push-pull capabilities of a surgeon (1DoF) that controls the guidewire in two bending planes (2DoF). The coil has limitations in working only along its X-axis. However, this simplifies control, especially for inexperienced surgeons. Moreover, the haptic interface allows the operator to make minor adjustments to the coil pose for additional control in case of potential misalignments.

D. Impact on Healthcare

We believe this system would be most helpful in hybrid ORs, thereby maximizing the benefits of the procedure in reduced time for the patients [32]. These rooms contain technologically advanced fluoroscopy and OR equipment. They also offer the ability to transition from MIS to open surgery if the situation requires it. The system is also suitable for use in conjunction with flexible tools embedded with magnetic particles, such as the magnetic soft continuum robots presented in Wang et al. [33] and Dreyfus et al. [34] and for untethered applications, such as capsule colonoscopies explained by Pittiglio et al. [35] and Norton et al. [36]. They exhibit similar diameters and magnetic strengths as the guidewire presented in this study. The system improves precision and dexterity in guidewire placement, reduces faulty assessments of vascular anatomy using pre-operative software, and accelerates stent implantations. This decreases failures, shortens intervention durations, and minimizes readmissions, resulting in improved intervention effectiveness for clinicians. In particular, mitigating CT exposure is crucial for reducing patient radiation dose. The system is designed to precisely navigate the guidewire to the appropriate location, reducing the need for repeated imaging and subsequent exposure. In addition, according to surgeon interviews, the system can potentially reduce the number of X-ray slices, as the surgeon does not have to validate the correct path to reach a fenestration constantly. Further quantification of this ability is needed for future studies.

V. CONCLUSION & FUTURE WORK

This study introduces a magnetic navigation system with a 7DoF robot arm and electromagnetic navigation tool that can reduce guidewire navigation times by 47%. User experience was evaluated through a questionnaire and interviews, showing positive results. The system follows a human-in-the-loop framework, allowing surgeons to remain active during the procedure, utilizing their expertise and judgment. The proposed framework will be expanded to incorporate real-time adjustments based on human operator feedback. Visual or auditory cues will be explored to enhance operator perception and improve performance. Moreover, non-invasive imaging techniques that provide high-resolution tissue structure images would enable surgeons to better understand anatomy for improved navigation and navigation safety in guidewire interventions. The integration of these advances is expected to expand the field of vascular stent implantation, making them safer and more efficient than current practices.

ACKNOWLEDGMENT

The authors would like to thank Mr. R. Liefers and Mr. J. Greve for their support with the Siemens Artis Pheno CT scanner. Medisch Spectrum Twente, Siemens Healthineers, and Flux Robotics B.V. supported this research, but had no role in its design, execution, analysis, or interpretation.

REFERENCES

- [1] R. N. Kitsis, J. A. Riquelme, and S. Lavandro, "Heart disease and cancer: Are the two killers colluding?," *Circulation*, vol. 138, no. 7, pp. 692–695, 2018.
- [2] J.-P. Becquemin et al., "A randomized controlled trial of endovascular aneurysm repair versus open surgery for abdominal aortic aneurysms in low-to moderate-risk patients," *J. Vasc. Surg.*, vol. 53, no. 5, pp. 1167–1173, 2011.
- [3] M. Kipling, A. Mohammed, and R. N. Medding, "Guidewires in clinical practice: Applications and troubleshooting," *Expert Rev. Med. Devices*, vol. 6, no. 2, pp. 187–195, 2009.
- [4] D. J. Arnaoutakis, M. Zammert, A. Karthikesalingam, and M. Belkin, "Endovascular repair of abdominal aortic aneurysms," *Best Pract. Res. Clin. Anaesthesiol.*, vol. 30, no. 3, pp. 331–340, 2016.
- [5] H. Rafii-Tari, C. J. Payne, and G.-Z. Yang, "Current and emerging robot-assisted endovascular catheterization technologies: A review," *Ann. Biomed. Eng.*, vol. 42, no. 4, pp. 697–715, 2014.
- [6] P. T. Campbell, K. R. Kruse, C. R. Kroll, J. Y. Patterson, and M. J. Esposito, "The impact of precise robotic lesion length measurement on stent length selection: Ramifications for stent savings," *Cardiovasc. Revascularization Med.*, vol. 16, no. 6, pp. 348–350, 2015.
- [7] W. B. Moskowicz and M. R. Ebeid, "Percutaneous management of challenging complex resistive targets in interventional pediatric cardiology," in *Debunking in Cardiovascular Interventions and Revascularization Strategies*. Amsterdam, The Netherlands: Elsevier, 2022, pp. 805–907.
- [8] M. A. Secretariat, "Endovascular repair of abdominal aortic aneurysm: An evidence-based analysis," *Ontario Health Technol. Assessment Ser.*, vol. 2, no. 1, pp. 1–46, 2002.
- [9] M. Hoekelmann, I. J. Rudas, P. Fiorini, F. Kirchner, and T. Haidegger, "Current capabilities and development potential in surgical robotics," *Int. J. Adv. Robot. Syst.*, vol. 12, no. 5, 2015, Art. no. 61.
- [10] G. Weisz et al., "Safety and feasibility of robotic percutaneous coronary intervention: Precise (percutaneous robotically-enhanced coronary intervention) study," *J. Amer. College Cardiol.*, vol. 61, no. 15, pp. 1596–1600, 2013.
- [11] N. R. Smilowitz et al., "Robotic-enhanced PCI compared to the traditional manual approach," *J. Invasive Cardiol.*, vol. 26, no. 7, pp. 318–321, 2014.
- [12] A. Stevenson, A. Kirresh, M. Ahmad, and L. Candilio, "Robotic-assisted PCI: The future of coronary intervention?," *Cardiovasc. Revascularization Med.*, vol. 35, pp. 161–168, 2022.
- [13] N. H. Dhanani et al., "The evidence behind robot-assisted abdominopelvic surgery: A systematic review," *Ann. Intern. Med.*, vol. 174, no. 8, pp. 1110–1117, 2021.
- [14] B. L. Nguyen, J. L. Merino, and E. S. Gang, "Remote navigation for ablation procedures—A new step forward in the treatment of cardiac arrhythmias," *Eur. Cardiol.*, vol. 6, no. 3, pp. 50–56, 2010.
- [15] C. Fischer, Q. Boehler, and B. J. Nelson, "Using magnetic fields to navigate and simultaneously localize catheters in endoluminal environments," *IEEE Robot. Automat. Lett.*, vol. 7, no. 3, pp. 7217–7223, Jul. 2022.
- [16] S. Gervasoni et al., "Magnetically assisted robotic fetal surgery for the treatment of spina bifida," *IEEE Trans. Med. Robot. Bionics*, vol. 4, no. 1, pp. 85–93, Feb. 2022.
- [17] B. S. Peters, P. R. Armijo, C. Krause, S. A. Choudhury, and D. Oleynikov, "Review of emerging surgical robotic technology," *Surg. Endoscopy*, vol. 32, no. 4, pp. 1636–1655, 2018.
- [18] C. M. Heunis, Y. P. Wotte, J. Sikorski, G. P. Furtado, and S. Misra, "The armm system-autonomous steering of magnetically-actuated catheters: Towards endovascular applications," *IEEE Robot. Automat. Lett.*, vol. 5, no. 2, pp. 705–712, Apr. 2020.
- [19] L. B. Kratchman, T. L. Bruns, J. J. Abbott, and R. J. Webster, "Guiding elastic rods with a robot-manipulated magnet for medical applications," *IEEE Trans. Robot.*, vol. 33, no. 1, pp. 227–233, Feb. 2017.
- [20] A. W. Mahoney and J. J. Abbott, "Five-degree-of-freedom manipulation of an untethered magnetic device in fluid using a single permanent magnet with application in stomach capsule endoscopy," *Int. J. Robot. Res.*, vol. 35, no. 1–3, pp. 129–147, 2016.
- [21] J. Qiu et al., "Guidewire simulation of endovascular intervention: A systematic review," *Int. J. Med. Robot. Comput. Assist. Surg.*, vol. 18, no. 6, 2022, Art. no. e2444.
- [22] C. M. Heunis, J. Sikorski, G. P. Furtado, and S. Misra, "The armm system: Demonstrating clinical feasibility in steering magnetically actuated catheters in endovascular applications," in *Proc. IEEE/RSJ Int. Conf. Intell. Robots Syst.*, 2019, Art. no. 3360.
- [23] E. Theodorou, J. Buchli, and S. Schaal, "Learning policy improvements with path integrals," in *Proc. 13th Int. Conf. Artif. Intell. Statist.*, 2010, vol. 9, pp. 828–835.
- [24] J. Sikorski, C. M. Heunis, F. Franco, and S. Misra, "The ARMM system: An optimized mobile electromagnetic coil for non-linear actuation of flexible surgical instruments," *IEEE Trans. Magn.*, vol. 55, no. 9, Sep. 2019, Art. no. 5600109.
- [25] F. Conti, F. Barbagli, D. Morris, and C. Sewell, "Chai 3D: An open-source library for the rapid development of haptic scenes," in *Proc. IEEE World Haptics*, 2005, pp. 21–29.
- [26] S. Chiaverini, B. Siciliano, and O. Egeland, "Review of the damped least-squares inverse kinematics with experiments on an industrial robot manipulator," *IEEE Trans. Control Syst. Technol.*, vol. 2, no. 2, pp. 123–134, Jun. 1994.
- [27] S. Zhang et al., "Design and characteristics of 3D magnetically steerable guidewire system for minimally invasive surgery," *IEEE Robot. Automat. Lett.*, vol. 7, no. 2, pp. 4040–4046, Apr. 2022.
- [28] J. Hwang et al., "An electromagnetically controllable microrobotic interventional system for targeted, real-time cardiovascular intervention," *Adv. Healthcare Mater.*, vol. 11, 2022, Art. no. 2102529.
- [29] Y. Kim, G. A. Parada, S. Liu, and X. Zhao, "Ferromagnetic soft continuum robots," *Sci. Robot.*, vol. 4, no. 33, 2019, Art. no. eaax7329.
- [30] K. MacPhedran and E. Hillebrand, "Cardiovascular and thoracic interventions," *Essentials Cardiopulmonary Phys. Ther. -E-Book*, Elsevier, vol. 8, 2016, Art. no. 375.
- [31] M. Niccolini, V. Castelli, C. Diversi, B. Kang, F. Mussa, and E. Sinibaldi, "Development and preliminary assessment of a robotic platform for neuroendoscopy based on a lightweight robot," *Int. J. Med. Robot. Comput. Assist. Surg.*, vol. 12, no. 1, pp. 4–17, 2016.
- [32] H. Jin and J. Liu, "Application of the hybrid operating room in surgery: A systematic review," *J. Invest. Surg.*, vol. 35, no. 2, pp. 378–389, 2022.
- [33] L. Wang, D. Zheng, P. Harker, A. B. Patel, C. F. Guo, and X. Zhao, "Evolutionary design of magnetic soft continuum robots," *Proc. Nat. Acad. Sci.*, vol. 118, no. 21, 2021, Art. no. e2021922118.
- [34] R. Dreyfus, Q. Boehler, and B. J. Nelson, "A simulation framework for magnetic continuum robots," *IEEE Robot. Automat. Lett.*, vol. 7, no. 3, pp. 8370–8376, Jul. 2022.
- [35] G. Pittiglio et al., "Magnetic levitation for soft-tethered capsule colonoscopy actuated with a single permanent magnet: A dynamic control approach," *IEEE Robot. Automat. Lett.*, vol. 4, no. 2, pp. 1224–1231, Apr. 2019.
- [36] J. C. Norton et al., "Intelligent magnetic manipulation for gastrointestinal ultrasound," *Sci. Robot.*, vol. 4, no. 31, 2019, Art. no. eaav7725.